IN-70 CR
260651
55P.

SIPHON FLOWS IN ISOLATED MAGNETIC FLUX TUBES

III. THE EQUILIBRIUM PATH OF THE FLUX TUBE ARCH

John H. Thomas

Department of Mechanical Engineering, Department of Physics and

Astronomy, and C. E. K. Mees Observatory

University of Rochester

and

NAG5-934

Benjamin Montesinos

Department of Theoretical Physics,

University of Oxford, England

ABSTRACT

The arched equilibrium path of a thin magnetic flux tube in a

plane-stratified, nonmagnetic atmosphere is calculated for cases in which the

flux tube contains a steady siphon flow. The large-scale mechanical

equilibrium of the flux tube involves a balance among the magnetic buoyancy

force, the net magnetic tension force due to the curvature of the flux–tube

axis, and the inertial (centrifugal) force due to the siphon flow along curved

streamlines. The ends of the flux tube are assumed to be pinned down by

some other external force. Both isothermal and adiabatic siphon flows are

considered for flux tubes in an isothermal external atmosphere. For the

isothermal case, in the absence of a siphon flow the equilibrium path reduces

to the static arch calculated by Parker (1975, 1979). The presence of a

siphon flow causes the flux tube arch to bend more sharply, so that magnetic

tension can overcome the additional straightening effect of the inertial force,

and reduces the maximum width of the arch. The curvature of the arch

increases as the siphon flow speed increases. For a critical siphon flow, with

supercritical flow in the downstream leg, the arch is asymmetric, with greater

curvature in the downstream leg of the arch. Adiabatic flows have

qualitatively similar effects, except that adiabatic cooling reduces the buoyancy

of the flux tube and thus leads to significantly wider arches. In some cases the

cooling is strong enough to create negative buoyancy along sections of the

flux tube, requiring upward curvature of the flux tube path along these sections and sometimes leading to unusual equilibrium paths of periodic, sinusoidal form.

Subject headings: hydromagnetics — plasmas — Sun: atmospheric motions — Sun: magnetic fields — Sun: sunspots

I. INTRODUCTION

In the two previous papers in this series (Thomas 1988, hereafter called Paper I; Montesinos and Thomas 1989, hereafter called Paper II) we explored the phenomenon of a siphon flow in a thin, isolated, arched magnetic flux tube in a stratified atmosphere under gravity. In those papers we ignored the problem of determining the equilibrium path of the flux tube in the atmosphere; instead, we assumed a shape for the flux–tube arch and then calculated the possible siphon flows along the flux tube. Now we relax that assumption and turn to the full problem of determining the exact equilibrium path of an arched flux tube containing a siphon flow. The siphon flow affects the equilibrium path of the flux tube by introducing inertial forces due to curvature of the flow streamlines and by altering the magnetic tension along the flux tube.

The problem of determining the equilibrium path of a static, thin, isolated magnetic flux tube in a plane–stratified atmosphere was first solved by Parker (1975, 1979). He considered the cases where the external atmosphere is either isothermal or polytropic and, in both cases, he took the temperatures inside and outside the flux tube to be equal. He found equilibrium paths h(x) (height h as a function of horizontal distance x) in the form of a symmetric arch, provided the footpoints of the arch are anchored by some other force. In the equilibrium configuration, the magnetic buoyancy

of the flux tube is balanced everywhere along the tube by the net magnetic tension force due to the curvature of the flux tube axis. This curvature is everywhere concave downward ($d^2h/dx^2 < 0$) in order to balance the upward buoyant force; thus, as we move away from the top of the arch, at some point the flux tube becomes vertical, beyond which the buoyant force cannot be balanced. This results in a limiting, maximum width of the flux tube arch, which works out to be equal to a few density scale heights of the external atmosphere.

In the present paper we show that arched equilibrium paths also exist for thin flux tubes containing a siphon flow. As far as the equilibrium path of the flux tube is concerned, the most important new feature introduced by the flow is the inertial force (centrifugal force) due to flow along curved streamlines. The net magnetic tension force must balance this inertial force in addition to the buoyancy force, which requires that the arch have greater curvature than in the static case. This leads to a somewhat smaller maximum width of the arch. The siphon flow also affects the shape of the arch by altering the magnetic field strength along the tube through the Bernoulli effect (decreased internal gas pressure). A brief mention of these results has already been given elsewhere (Thomas 1989; Thomas and Montesinos 1989).

Spruit (1981) has given a derivation of the equations describing the equilibrium path of a thin flux tube, using a method different from Parker's.

Browning and Priest (1984, 1986) extended the work of Parker and Spruit by considering the effect of adding an ambient magnetic field to the external atmosphere.

As in Papers I and II, the atmosphere outside the flux tube is assumed to be a plane–stratified, isothermal, perfect–gas atmosphere in hydrostatic equilibrium. The subscript e will be used to denote quantities associated with the external atmosphere. Letting T_{e0} denote the uniform exterior temperature, the distributions of pressure and density with height h outside the flux tube are given by

$$p_e = p_{e0}\exp(-h/H) \quad , \quad \rho_e = \rho_{e0}\exp(-h/H) \quad , \tag{1.1}$$

where $H = RT_{e0}/g$ is the constant scale height and p_{e0} and ρ_{e0} are the reference external pressure and density at $h = 0$.

The main purpose of this paper is to show how the equilibrium path of a thin, isolated magnetic flux tube in a stratified atmosphere can be calculated in cases where the flux tube contains a siphon flow and to illustrate the effect of the siphon flow on the path of the flux tube. For this purpose, our assumption of a simple isothermal external atmosphere is sufficient. In a subsequent paper in this series we will adopt a more realistic models of the solar convection zone and photosphere as the external atmosphere in order to relate our siphon flow calculations more directly to intense magnetic flux

tubes on the Sun.

Note: After this paper was submitted for publication, a paper by Degenhardt (1989) appeared in which he also solves for the equilibrium path of a thin, isolated magnetic flux tube containing a siphon flow, using essentially the same method we present here. Other than the basic method, however, there is little overlap in the two papers. Degenhardt concentrates on specific, dimensional cases in a more detailed plane–stratified model of the external solar atmosphere, whereas we have emphasized an exploration of the full range of parameter values for a simple external atmosphere (isothermal). Degenhardt considers only isothermal flows, whereas we consider both isothermal and adiabatic flows. Also, Degenhardt does not integrate the governing equations down to the point where the flux tube becomes vertical and thus does not determine the maximum width of the arch as we do here. Degenhardt shows that in the case of a temperature–stratified (nonisothermal) external atmosphere, a smooth transition from subcritical to supercritical flow can sometimes occur in the ascending part of the flux tube arch, whereas in an isothermal external atmosphere such a transition can occur only at the top of the arch.

II. BASIC EQUATIONS

Our derivation of the basic equations describing the equilibrium path of a thin flux tube containing a siphon flow generally follows the approach of

Spruit (1981). The momentum equation for steady flow is

$$\rho \mathbf{v} \cdot \nabla \mathbf{v} = -\nabla (p + \frac{B^2}{8\pi}) + \frac{1}{4\pi} \mathbf{B} \cdot \nabla \mathbf{B} + \rho \mathbf{g} \; . \tag{2.1}$$

The flux tube is in lateral pressure balance with the external atmosphere:

$$p + \frac{B^2}{8\pi} = p_e \; . \tag{2.2}$$

(The subscript e denotes quantities associated with the external atmosphere, while unsubscripted variables refer to the interior of the flux tube.) Then, assuming hydrostatic equilibrium of the external atmosphere, we can write

$$\nabla (p + \frac{B^2}{8\pi}) = \nabla p_e = \rho_e \mathbf{g} \; ,$$

and the momentum equation (2.1) can be written in the form

$$\rho \mathbf{v} \cdot \nabla \mathbf{v} = \frac{1}{4\pi} \mathbf{B} \cdot \nabla \mathbf{B} + (\rho - \rho_e) \mathbf{g} \; . \tag{2.3}$$

We assume that the flux tube is thin, in the sense that its radius is much smaller than either its radius of curvature or the scale height H of the external atmosphere. Then we can consider the flow in the interior of the flux tube to be one-dimensional, i. e., locally parallel and uniform across the cross–section of the flux tube, so that all interior variables are functions only of the tangential coordinate s. Let $\boldsymbol{\sigma}$ denote the unit vector along the axis of the flux tube (in the s–direction) and let $\mathbf{v}$ denote the unit vector normal to the axis of the flux tube, directed toward the center of curvature (see Fig. 1). Then we decompose the magnetic tension force into tangential and normal

components as follows:

$$\mathbf{B \cdot \nabla B} = B \frac{d}{ds}(B\sigma) = (B\frac{dB}{ds})\sigma + B^2\frac{d\sigma}{ds} = (\frac{1}{2}\frac{dB^2}{ds})\sigma + B^2\mathbf{k} \ , \qquad (2.4)$$

where $\mathbf{k} = d\sigma/ds = \mathbf{v}/R$ is the radius of curvature vector, with R denoting the

radius of curvature of the flux tube axis. Similarly, for the inertial force we

can write

$$\mathbf{v \cdot \nabla v} = (\frac{1}{2}\frac{dv^2}{ds})\sigma + v^2\mathbf{k} \ . \qquad (2.5)$$

The acceleration of gravity $\mathbf{g}$ can also be decomposed into tangential and

normal components, in the form

$$\mathbf{g} = (-g\sin\theta)\sigma + (g\cos\theta)R\mathbf{k} \ , \qquad (2.6)$$

where θ is the angle between the flux tube axis and the horizontal direction

(see Fig. 1). Using expressions (2.4) – (2.6), we can write the σ and $\mathbf{k}$

components of equation (2.3) as follows:

$$\rho \frac{d}{ds}(\frac{v^2}{2}) - \frac{d}{ds}(\frac{B^2}{8\pi}) - (\rho_e - \rho)g\sin\theta = 0 \ , \qquad (2.7)$$

$$\frac{1}{R}(\rho v^2 - \frac{B^2}{4\pi}) + (\rho_e - \rho)g\cos\theta = 0 \ . \qquad (2.8)$$

The tangential component, equation (2.7), describes the siphon flow in the flux

tube and, as we shall show below, is equivalent to the momentum equation

used in Papers I and II. The normal component, equation (2.8), describes the

large–scale mechanical equilibrium of the flux tube; it represents a balance

among the inertial force $\rho v^2/R$ due to the curvature of the flow streamlines,

the magnetic tension force $-B^2/4\pi R$ due to the curvature of the flux tube, and

the normal component $(\rho_e - \rho)g \cos\theta$ of the buoyancy force.

If we let h(x) denote the height of the flux tube axis (see Fig. 1), then we can

write

$$\frac{dh}{dx} = \tan\theta \quad , \quad \frac{d^2h}{dx^2} = \frac{1}{\cos^2\theta}\frac{d\theta}{dx} \quad ,$$

$$\frac{1}{R} = \frac{-\dfrac{d^2h}{dx^2}}{\left[1 + (\dfrac{dh}{dx})^2\right]^{3/2}} = -\cos\theta\frac{d\theta}{dx} \quad .$$

With these relations, we can formulate the problem of finding the equilibrium

path h(x) of the flux tube, based on equation (2.8), as a pair of coupled

first-order differential equations for $\theta(x)$ and h(x):

$$\frac{dh}{dx} = \tan\theta \, , \qquad\qquad (2.9)$$

$$(\frac{B^2}{4\pi} - \rho v^2)\frac{d\theta}{dx} = -(\rho_e - \rho)g \, . \qquad\qquad (2.10)$$

These two equations together with the pair of first-order differential

equations for the velocity v and cross-sectional area A of the siphon flow

(derived in Papers I and II) and the condition of magnetic flux conservation, AB

= constant, provide a set of equations for determining simultaneously the

siphon flow inside an arched flux tube and the equilibrium path h(x) of the flux

tube.

The tangential component of the steady momentum equation can be written

in the form

$$\rho v \frac{dv}{ds} = -\frac{dp}{ds} - \rho g \frac{dh}{ds} , \qquad (2.11)$$

noting that $\sin\theta = dh/ds$. Equation (2.11), which is the form of the momentum

equation used to describe the one–dimensional siphon flows in Papers I and

II, follows directly from equation (2.1), and also follows from equation (2.7) if

we again make use of the condition of lateral pressure balance, equation

(2.2), and the hydrostatic equation for the external atmosphere, $\nabla p_e = \rho_e g$. To

complete the description of the one–dimensional steady siphon flow within the

flux tube, we also need the equation of mass conservation,

$$\frac{d}{ds}(\rho v A) = 0 \quad , \quad \rho v A = Q = \text{constant}, \qquad (2.12)$$

the equation of magnetic flux conservation,

$$\frac{d}{ds}(AB) = 0 \quad , \quad AB = \Phi = \text{constant} , \qquad (2.13)$$

the equation of state,

$$p = \rho RT , \qquad (2.14)$$

and the appropriate energy equation,

$$\text{isothermal flow: } T = T_e \quad , \quad \text{adiabatic flow: } \frac{p}{p_0} = \left(\frac{\rho}{\rho_0}\right)^\gamma . \qquad (2.15)$$

Equations (2.11) – (2.15), together with equation (2.2), constitute the complete

set of equations describing the siphon flow, as used in Papers I and II. As

before, we are using the isothermal and adiabatic cases to represent

extremes between which the behavior of a flow with a more realistic energy

equation (including radiative exchange) will lie.

It is convenient to write the basic equations in terms of dimensionless quantities. We adopt the same scaling as in Papers I and II, except that here we use the scale height H of the external atmosphere as the length scale for both the height h and the horizontal distance x. In Papers I and II, the horizontal distance x was scaled by the distance L between the footpoints of the arch, and L was left undetermined. Here it is more convenient to use the same scaling for h and x, so that dimensionless plots of h(x) show the actual shape of the flux tube arch. The actual value of the distance L between footpoints is determined by the equilibrium solution for h(x). Also, here we take the origin x = 0 to be at the point where the arch reaches its maximum height (see Fig. 1), whereas in Papers I and II the origin was taken to be at the left footpoint of the arch (where h = 0).

Using H as the length scale and the exterior isothermal sound speed $c_i = (RT_{e0})^{1/2}$ as the velocity scale, we define the following dimensionless quantities (denoted by an overbar):

$$\bar{x} = \frac{x}{H} \ , \ \bar{h} = \frac{h}{H} \ , \ \bar{p} = \frac{p}{p_0} \ , \ \bar{\rho} = \frac{\rho}{\rho_0} \ , \ \bar{T} = \frac{T}{T_0} \ , \ \bar{A} = \frac{A}{A_0} \ , \ \bar{B} = \frac{B}{B_0} \ ,$$

$$\bar{v} = \frac{v}{c_i} \ , \ \bar{v}_0 = \frac{v_0}{c_i} \ , \ \bar{c} = \frac{c}{c_i} \ , \ \bar{a} = \frac{a}{c_i} \ , \ \bar{c}_t = \frac{c_t}{c_i} \ , \ \bar{c}_1 = \frac{c_1}{c_i} \ , \tag{2.16}$$

where p_0, ρ_0, T_0, A_0, B_0, and v_0 are the reference values (at h = 0 at the upstream footpoint) of the pressure p, density ρ, temperature T, cross–sectional area A, magnetic field strength B, and velocity v inside the flux

tube. The Alfvén speed a, the "tube speed" c_t, and the characteristic speed c_1 are defined by

$$a^2 = \frac{B^2}{4\pi\rho} \quad , \quad c_t^2 = \frac{c^2 a^2}{c^2 + a^2} \quad , \quad c_1^2 = \left(\frac{\rho_e - \rho}{\rho_e}\right) c^2 \quad , \tag{2.17}$$

as in Papers I and II. The sound speed c inside the flux tube is taken to be the isothermal sound speed $(RT)^{1/2}$ for isothermal flow and the adiabatic sound speed $(\gamma RT)^{1/2}$ for adiabatic flow. We also define the "plasma beta" based on the external pressure as follows:

$$\beta(\bar{h}) \equiv \frac{8\pi p_e(\bar{h})}{B^2(\bar{h})} \quad , \quad \beta_0 \equiv \beta(0) = \frac{8\pi p_{e0}}{B_0^2} \quad , \tag{2.18}$$

where β_0 (called simply β in Papers I and II) is the particular value of β at $\bar{h} = 0$. In terms of β, the lateral pressure balance condition (2.2) may be expressed as

$$\frac{p}{p_e} = \frac{\beta - 1}{\beta} \quad . \tag{2.19}$$

III. ISOTHERMAL FLOWS

In this section we consider isothermal flows, for which the temperature inside the flux tube is everywhere equal to the uniform external temperature,

i. e., $T = T_{e0} =$ constant. In this case the condition of lateral pressure balance, equation (2.2), allows us to express the buoyancy term on the right hand side of equation (2.10) as

$$- (\rho_e - \rho)g = - \frac{g}{RT_{e0}} (p_e - p) = - \frac{1}{H} (\frac{B^2}{8\pi}) \; . \tag{3.1}$$

Then, in terms of the nondimensional variables defined in equations (2.16) and (2.17), the pair of equations (2.9) and (2.10) can be written in the form

$$\frac{d\overline{h}}{d\overline{x}} = \tan\theta \; , \tag{3.2}$$

$$\left[(\frac{2}{\beta_0 - 1}) \overline{B}^2 - \overline{\rho} \overline{v}^2 \right] \frac{d\theta}{d\overline{x}} = - (\frac{1}{\beta_0 - 1}) \overline{B}^2 \; , \tag{3.3}$$

As shown in Paper I, the set of equations (2.2) and (2.11) – (2.15) in the case of isothermal flow lead to the velocity–height relation

$$\frac{d\overline{v}}{d\overline{x}} = \overline{v} \left\{ \frac{1}{2 - \overline{v}^2 [\beta_0 \overline{A}^2 \exp(- \overline{h}) + 1]} \right\} \frac{d\overline{h}}{d\overline{x}} \tag{3.4}$$

and the area–height relation

$$\frac{d\overline{A}}{d\overline{x}} = \overline{A} \left\{ \frac{1 - \overline{v}^2 \beta_0 \overline{A}^2 \exp(-\overline{h})}{2 - \overline{v}^2 [\beta_0 \overline{A}^2 \exp(-\overline{h}) + 1]} \right\} \frac{d\overline{h}}{d\overline{x}} \quad . \tag{3.5}$$

Equations (3.2) – (3.5), together with the simple condition of magnetic flux

concentration, $\overline{A}\overline{B} = 1$, constitute a coupled set of nonlinear equations for

determining simultaneously the siphon flow variables $\overline{v}(\overline{x})$ and $\overline{A}(\overline{x})$ and the

equilibrium path $\overline{h}(\overline{x})$ of the flux tube. However, computationally the problem

is actually decoupled in the sense that equations (3.4) and (3.5) can be written

with height $\overline{h}$ as the independent variable:

$$\frac{d\overline{v}}{d\overline{h}} = \overline{v} \left\{ \frac{1}{2 - \overline{v}^2 [\beta_0 \overline{A}^2 \exp(-\overline{h}) + 1]} \right\} \quad , \tag{3.6}$$

$$\frac{d\overline{A}}{d\overline{h}} = \overline{A} \left\{ \frac{1 - \overline{v}^2 \beta_0 \overline{A}^2 \exp(-\overline{h})}{2 - \overline{v}^2 [\beta_0 \overline{A}^2 \exp(-\overline{h}) + 1]} \right\} \quad . \tag{3.7}$$

Thus, we can solve for the flow variables $\overline{v}(\overline{h})$ and $\overline{A}(\overline{h})$ using equations (3.6)

and (3.7), subject to imposed values at some height $\overline{h}$. The other flow

variables $\overline{\rho}$, $\overline{p}$, $\overline{T}$, and $\overline{B}$ are then given as functions of $\overline{h}$ by using equations

(2.12) – (2.15). We can then solve equations (3.2) and (3.3) for the equilibrium

path $\overline{h}(\overline{x})$ of the flux tube using the known quantities $\overline{v}(\overline{h})$, $\overline{B}(\overline{h})$, and $\overline{p}(\overline{h})$. (We

should point out that this decoupling of the problem is a direct consequence of

the thin flux tube approximation; in a thick flux tube, the flow will not be

one-dimensional and the problem of determining the equilibrium path and the flow will be fully coupled.)

In order to solve for both the siphon flow and the equilibrium path, we proceed as follows. We choose a value of β_0 and specify the nondimensional height α of the arch above the reference level $\bar{h} = 0$. Then we can determine the siphon flow variables by integrating equations (3.6) and (3.7) beginning at $\bar{h} = 0$, where we have the specified initial values $\bar{v}(0) = \bar{v}_0$, $\bar{A}(0) = 1$. We use a fourth-order Runge-Kutta method with variable mesh spacing (Press *et al.* 1986) for the numerical integration. Once the siphon flow is determined up to the top of the arch and we know $\bar{v}(\bar{h})$ and $\bar{B}(\bar{h})$, equations (3.2) and (3.3) can be integrated starting from the top of the arch, where we also have the known initial conditions $\bar{h} = \alpha$, $\theta = 0$. Also, we can take the values of $\bar{v}$ and $\bar{A}$ at the top of the arch determined by the numerical integration of equations (3.6) and (3.7) and use them as initial values for the equations ((3.4) and (3.5). In this way, the full set of four equations (3.2) – (3.5), with the condition $\bar{A}\bar{B} = 1$, can be integrated simultaneously, beginning at the top of the arch (at $\bar{x} = 0$), in order to determine $\bar{h}(\bar{x})$, $\bar{v}(\bar{x})$, $\bar{A}(\bar{x})$, and $\bar{B}(\bar{x})$, and hence all other flow variables. The integration can be carried beyond the point where $\bar{h} = 0$, since the choice of the reference level $\bar{h} = 0$ is arbitrary. The integration can proceed up to the point where the flux tube becomes vertical, i. e., where

$d\bar{h}/d\bar{x}$ becomes infinite. This yields a full solution of the problem for the parameter values α, β_0, and $\bar{v}_0$. We are free to choose any other height (below the top of the arch) as the reference level $\bar{h} = 0$ for this solution, in which case the solution corresponds to a different arch height α and different values of $\beta_0 = \beta(0)$ and $\bar{v}_0 = \bar{v}(0)$. In fact, we could just begin by specifying the values of $\bar{v}$, $\bar{A}$, and β at the top of the arch and integrate equations (3.2) – (3.5) from there, but the method we have chosen is more consistent with our approach in Papers I and II.

In the absence of a siphon flow ($\bar{v} = 0$), the pair of equations (3.2) and (3.3) for determining the path $\bar{h}(\bar{x})$ of the flux tube reduce to

$$\frac{d\bar{h}}{d\bar{x}} = \tan\theta \quad , \quad \frac{d\theta}{d\bar{x}} = -\frac{1}{2} \; . \tag{3.8}$$

These equations are equivalent to those solved by Parker (1975, 1979) and have the analytical solution

$$\tan^2(\bar{x}/2) = \exp(\alpha - \bar{h}) - 1 \tag{3.9}$$

for the case where $\bar{h} = \alpha$ when $\bar{x} = 0$. The resulting arch shape $\bar{h}(\bar{x})$ is shown in Figure 2a (*dot–dash curve*), where we have taken $\alpha = 1.0$. Note that $\bar{h} \rightarrow -\infty$ as $\bar{x} \rightarrow \pm \pi$, so that the arch has a limiting maximum width $L_{max} = 2\pi H$. Note also that in the static isothermal case, the equilibrium path is independent of the value of β_0 , i. e., independent of the magnetic field strength of the tube.

This is due to the fact that each of the two competing forces, the magnetic buoyancy and the net magnetic tension, scale as B^2. With a siphon flow, however, the added inertial force does not scale simply as B^2 and the equilibrium path does depend on β_0 (see equations (3.2) and (3.3)).

In addition to the static case, Figure 2a shows examples of the computed equilibrium path of the flux tube for two subcritical siphon flows and the critical siphon flow (with both subcritical and supercritical downstream branches) for the parameter values $\alpha = 1.0$ and $\beta_0 = 3.0$. The corresponding distributions of velocity $\bar{v}(\bar{x})$, cross–sectional area $\bar{A}(\bar{x})$, and plasma beta $\beta(\bar{x})$ for these flows are also shown in Figure 2. Note in Figure 2c that the critical flow produces bulge points (points of local maximum cross-sectional area) in the flux tube (see Paper I for a discussion of these bulge points). In Figure 2d we see that the flow reduces the value of $\beta(\bar{x})$ (i. e., increases the magnetic field strength), compared to the static case, everywhere above $h = 0$. This is a consequence of the decreased internal pressure associated with the siphon flow (the Bernoulli effect). Here we have taken the value of β to be 3.0 at $h = 0$ in all four cases (the static case and the three cases with siphon flows). To see the effect of the siphon flow on an individual flux tube of fixed total magnetic flux, it is more appropriate to take the limiting value of β as $h \to -\infty$ (where $v \to 0$) to be the same in all cases; then the siphon flow will reduce the value of β

below that of the static tube everywhere along the tube.

Comparing the different curves of $\bar{h}(\bar{x})$ in Figure 2a, we see that for fixed β_0 increasing the siphon flow speed causes the flux tube to bend more sharply, in order that the net magnetic tension force can balance the sum of the inertial and buoyancy forces. The siphon flow thus reduces the maximum width of the arch below the value for the static arch. For example, in Figure 2a the critical flow with its subcritical downstream branch reduces the maximum width of the arch to $L_{max} = 5.31H$, compared to $L_{max} = 2\pi H = 6.28H$ in the static case. For the case of the critical flow with its supercritical downstream branch, the equilibrium path is asymmetric, with greater curvature in the supercritical downstream leg of the arch and a further reduction of the maximum width. Of course, the flow will not actually follow the supercritical branch all the way to the downstream footpoint; at some point in the downstream branch the flow will decelerate to subcritical speed through a standing tube shock and the curvature will be reduced beyond that point. We intend to present computations of critical flows with standing tube shocks in a subsequent paper in this series.

The purely subcritical steady flows we present here (and in the next section) are all symmetric about the top of the arch and, in particular, the gas pressure is the same at both footpoints. If we were to add the effects of

viscosity, these subcritical flows would no longer be symmetric; the steady

flow would require a smaller pressure at the downstream footpoint in order

to balance the viscous stresses. There is no ambiguity about the symmetric,

steady subcritical flows in the inviscid case, however, as suggested by

Degenhardt (1989). These flows simply represent the steady-state limit of a

transient flow that arises as a consequence of an initial pressure difference

between the two footpoints, with the flow directed toward the lower-pressure

footpoint. The critical inviscid flows with supercritical flow in the downstream

leg of the arch are inherently asymmetric, although they too could have equal

pressures at the two footpoints with a tube shock of suitable strength in the

downstream leg.

In Figure 3 we show the equilibrium path $\bar{h}(\bar{x})$, velocity $\bar{v}(\bar{x})$, and

cross-sectional area $\bar{A}(\bar{x})$ for critical flows with three different values of β_0

(2.0, 3.0, and 6.0), all with $\alpha = 1.0$, along with the static case for comparison.

For each critical flow both the subcritical and supercritical downstream

branches are shown. Note that for increasing β_0, i. e., for decreasing

magnetic field strength, the critical siphon flow has greater effect on the

equilibrium path of the arch (produces greater curvature), even though the

flow speeds are lower for increasing β_0. In Figure 3a, the maximum width of

the arch, based on the subcritical downstream branch of the flow, is $L_{max} =$

5.68H, 5.31H, and 4.67H for the critical flows with $\beta_0 = 2.0$, 3.0, and 6.0

respectively, which can be compared to the value $L_{max} = 6.28H$ for the static

case. The width of the arch is even further reduced for supercritical

downstream branches of the flows, but again in these cases the flow must

decelerate abruptly to subcritical speed somewhere in the downstream

branch across a standing tube shock, which we have not computed here.

IV. ADIABATIC FLOWS

Our treatment of adiabatic siphon flows follows the notation of Paper II. We

use the second form of the energy equation (2.15), and we allow the

temperatures T_0 and T_{e0} inside and outside the flux tube at the upstream

footpoint to be different, letting $\tau = (T_0/T_{e0})$ denote their ratio. Equations (2.9)

and (2.10) for the equilibrium path can be written in the form

$$\frac{d\bar{h}}{d\bar{x}} = \tan\theta \ , \tag{4.1}$$

$$\left[(\frac{2\tau}{\beta_0-1})\bar{B}^2 - \bar{\rho}\,\bar{v}^2 \right] \frac{d\theta}{d\bar{x}} = -\left[(\frac{\beta_0\tau}{\beta_0-1})\exp(-\bar{h}) - \bar{\rho} \right] \ , \tag{4.2}$$

where we have also made use of equation (1.1). As shown in Paper II, the set

of equations (2.2) and (2.11) – (2.15) lead to the coupled equations

$$\frac{d\bar{v}}{d\bar{h}} = \bar{v}\left[\frac{\Gamma - \bar{c}^2}{\Gamma(\bar{c}_t^2 - \bar{v}^2)}\right] , \qquad (4.3)$$

$$\frac{d\bar{A}}{d\bar{h}} = \bar{A}\left[\frac{\bar{c}_1^2 - \bar{v}^2}{\Gamma(\bar{c}_t^2 - \bar{v}^2)}\right] , \qquad (4.4)$$

for the velocity and cross-sectional area, with

$$\Gamma = \left[\frac{2\gamma(\bar{c}^2 + \bar{a}^2)}{2\bar{c}^2 + \gamma\bar{a}^2}\right] , \quad \bar{c}^2 = \tau\gamma\bar{p}^{\gamma-1} , \quad \bar{a}^2 = \frac{2\tau}{(\beta_0 - 1)\bar{p}\,\bar{A}^2} ,$$

$$\bar{c}_t^2 = \frac{\bar{c}^2\bar{a}^2}{\bar{c}^2 + \bar{a}^2} , \quad \bar{c}_1^2 = \frac{(2\bar{c}^2 + \gamma\bar{a}^2 - 2\gamma)\bar{c}^2}{2\bar{c}^2 + \gamma\bar{a}^2} , \quad \bar{p} = \frac{\bar{v}_0}{\bar{v}\,\bar{A}} . \qquad (4.5)$$

(Note: Equation (3.8) of Paper II, which corresponds to equation (4.3) above, contains a misprint, and equation (4.3) above is the correct form of the velocity equation. The correct form of the equation was used for all of the calculations in Paper II and the results were not affected by the misprint.) Equations (4.3) and (4.4), together with the auxilliary relations (4.5), constitute a closed set of equations for the siphon flow as a function of height $\bar{h}$; they replace equations (3.6) and (3.7) used in the case of isothermal flow and can be integrated to determine the flow conditions at the top of the arch. If we rewrite them with $\bar{x}$ as the independent variable, equations (4.3) and (4.4)

together with equations (4.1) and (4.2) form a closed set of equations for

determining simultaneously the siphon flow and the equilibrium path $\bar{h}(\bar{x})$, by

integrating from the known initial conditions at the top of the arch.

For the adiabatic flows considered here, the limiting static case (for $\bar{V} = 0$)

corresponds to a flux tube with static adiabatic internal stratification,

embedded in the isothermal external atmosphere. The internal pressure,

density, and temperature in the static case are given by

$$\bar{p} = \left[1 - (\frac{\gamma-1}{\gamma\tau})\bar{h} \right]^{\frac{\gamma}{\gamma-1}} \quad , \quad \bar{\rho} = \left[1 - (\frac{\gamma-1}{\gamma\tau})\bar{h} \right]^{\frac{1}{\gamma-1}} \quad , \quad \bar{T} = \left[1 - (\frac{\gamma-1}{\gamma\tau})\bar{h} \right] \quad , \quad (4.6)$$

and the cross–sectional area and magnetic field strength are given by

$$\bar{A} = \left[\beta_0 \exp(-\bar{h}) - (\beta_0 - 1)\bar{p} \right]^{-\frac{1}{2}} \quad , \quad \bar{B} = \left[\beta_0 \exp(-\bar{h}) - (\beta_0 - 1)\bar{p} \right]^{\frac{1}{2}} \quad (4.7)$$

(see Paper II). Unlike the static isothermal tube, the static adiabatic tube has a

limiting maximum height $\bar{h}_{lim} = \gamma\tau/(\gamma-1)$ where the internal pressure, density,

and temperature go to zero; we are thus limited to considering arch heights

$\alpha < \bar{h}_{lim}$ (= 2.5 for $\tau = 1.0$ and $\gamma = 5/3$).

In a sense, the static adiabatic case is unrealistic for solar applications. It is

reasonable to consider a siphon flow to be nearly adiabatic if the flow speed is

so great that there isn't enough time for the internal gas to be heated to

thermal equilibrium by thermal conduction (or radiation) from the surroundings. If the radiative exchange time for the tube is much longer than the time it takes the flow to traverse the arch, then the flow will be nearly adiabatic and there will be significant cooling of the internal gas as it expands in the rising part of the arch. However, in the case of slow flows or, in the extreme, a static tube, heat exchange with the surroundings will be important and the primary justification for treating the flow as adiabatic does not apply. Nevertheless, the static adiabatic tube defined by equations (4.6) and (4.7) is a physically possible state if the flux tube were truly insulated from its surroundings and is also the correct mathematical limit of the adiabatic flow solutions for $\bar{v} \to 0$; as such, it needs to be understood.

In the adiabatic case (either static tube or with a siphon flow) the temperature inside the flux tube can be greater than or less than the temperature of the surrounding atmosphere, and this temperature difference can enhance or reduce the buoyancy of the flux tube. For example, in a static adiabatic tube with $\tau = 1.0$ the temperature inside the tube equals the external temperature only at the level $h = 0$; as we go above $h = 0$ the tube is progressively cooler than the surroundings, and as we go below $h = 0$ the tube is progressively hotter than the surroundings. In some cases the tube may reach a height (call it h') where the density increase due to adiabatic cooling completely offsets the density decrease due to the reduced internal

pressure (the magnetic buoyancy effect) and the tube becomes heavier than the surroundings above that height; then, the curvature of the tube must switch to being concave upward above the height h', and the point h = h' is an inflection point of the curve h(x). The relative effect of the adiabatic cooling is greater for larger values of β_0 because the magnetic buoyancy decreases with increasing β_0.

Figure 4 shows examples of the equilibrium path of a static adiabatic flux tube in an isothermal external atmosphere, computed from equations (4.1) and (4.2) with the appropriate static distributions of $\bar{p}$ and $\overline{B}$ given in equations (4.6) and (4.7). In Figure 4a we have plotted the paths $\bar{h}(\bar{x})$ of tubes with several values of β_0, but all with $\alpha = 1.0$ (same maximum height) and $\tau = 1.0$ (internal temperature equal to external temperature at $\bar{h} = 0$). Each flux tube is cooler than the surroundings everywhere above $\bar{h} = 0$ and hotter than the surroundings everywhere below $\bar{h} = 0$. As β_0 increases, the relative effect of the adiabatic internal stratification becomes more pronounced and the density in the upper part of the arch becomes more nearly equal to the external density; this is manifested in a reduced curvature of the arch, and the top part of the arch becomes progressively flatter for increasing β_0. Eventually β_0 reaches a value (somewhere between 4.5 and 5.0) where the density at the top of the arch is

exactly equal to the external density and the tube is neutrally buoyant there.

Then, with a further increase in β_0, the tube becomes heavier than the surroundings at the top of the arch and the arch must become concave upward there. The equilibrium solution then abruptly switches over to a curious, sinusoidal-like path, such as the paths shown for $\beta_0 = 5.0$ and 6.0 in Figure 4. In these cases, the negative buoyancy of the lower parts of the sinusoidal path (concave upward) is balanced by the positive buoyancy of the upper parts of the sinusoidal path (concave downward). There is positive buoyancy in the upper parts of the tube in these cases because, whereas the internal density is decreasing algebraically with height [cf. eqs (4.6)], the external density is decreasing exponentially [cf. eqs. (1.1)], so eventually a height is reached where the internal density is again lower than the external density and the buoyancy is again positive. Note that the sinusoidal flux tubes with $\beta_0 = 5.0$ and 6.0 in Figure 4 are everywhere cooler than their surroundings, since they don't extend down to $\bar{h} = 0$ where we have assumed $\tau = 1.0$. Also note that for these two flux tubes the values of $\beta_0 = \beta(0)$ are somewhat irrelevant because the tubes do not extend down to $\bar{h} = 0$; unlike the static isothermal case, β is not constant with height in a static adiabatic tube, but instead varies as

$$\beta(\bar{h}) = \frac{\beta_0 \exp(-\bar{h})}{\beta_0 \exp(-\bar{h}) - (\beta_0 - 1)\,[1 - (\frac{\gamma-1}{\gamma\tau})\bar{h}]^{\frac{\gamma}{\gamma-1}}} \quad , \tag{4.8}$$

which follows from equations (1.1), (4.6), and (4.7).

In Figure 4b we show the equilibrium paths of static adiabatic tubes with greater maximum height ($\alpha = 2.0$) than the tubes in Figure 4a. The behavior is similar, except that here there is an intermediate case (for $\beta_0 = 6.0$) with sections of upward concavity (negative buoyancy) on either side of the arch but with downward concavity (positive buoyancy) at the top of the arch. This situation is possible because the curves of internal density (algebraic) and external density (exponential) as functions of height will cross at two different heights for some range of values of the reference densities at $\bar{h} = 0$, provided the arch is high enough.

Figure 5 shows computed examples of the equilibrium path of a flux tube containing an adiabatic siphon flow, together with the velocity and cross sectional area along the tube, for the parameter values $\alpha = 1.0$, $\beta_0 = 3.0$, and τ = 1.0. Shown here are the static case (for $\bar{v}_0 = 0$), two examples of subcritical flow (for $\bar{v}_0 = 0.15$ and 0.25), and the critical flow (for $\bar{v}_0 = 0.316207$) with its subcritical and supercritical downstream branches. As in the isothermal case, we see that increasing the siphon flow speed increases the curvature of the flux tube and reduces the overall width of the arch. Here the overall width

of the arch is reduced from L = 8.94H in the static case to L = 7.11H in the case of the symmetric critical flow with its subcritical downstream branch (the long–dashed curve). Comparing Figure 5a with Figure 2a, we see that the adiabatic case produces wider arches than the isothermal case. The adiabatic cooling of the gas leads to greater internal densities (compared to the isothermal case) and hence a weaker buoyancy force, which in turn requires less curvature of the flux tube axis in order to establish mechanical equilibrium.

As expected, the critical adiabatic flow exhibits bulge points (Fig. 5c). The somewhat curious fact that the siphon flow speed (Fig. 5b) reaches a minimum and then begins to increase rapidly as we go down either leg of the arch is a consequence of the fact that the tube gets progressively hotter as we go lower down (because of the adiabatic assumption). Thus, the "local" value of the temperature ratio τ (as opposed to the fixed value $\tau = 1.0$ at $\bar{h} = 0$) increases with depth and eventually exceeds the critical value $\tau_2 \equiv [\gamma(\beta-1)+2]/\gamma\beta$ and there the flow behaves as in the "superheated" tubes discussed in Paper II (see the discussion in section IV and Fig. 9a of Paper II). Of course, it is unrealistic to apply the adiabatic assumption all the way down the arch as $\bar{h} \rightarrow -\infty$, so the large increase in velocity there is artificial.

In Figure 6 we show flux tubes with adiabatic siphon flows similar to those in

Figure 5, except with $\beta_0 = 6.0$ instead of 3.0. For the critical flow (with $\bar{v}_0 =$ 0.228438) and for the purely subcritical flow with $\bar{v}_0 = 0.2$, there is an equilibrium path in the typical form of an arch of limited width. However, if the initial velocity is further reduced to $\bar{v}_0 = 0.15$, there is no longer an arched equilibrium path extending downward without limit. Instead, the integration of the basic equations away from the center $\bar{x} = 0$ gives a sinusoidal–shaped equilibrium path, as does the static case ($\bar{v}_0 = 0$). Here we have a case of a flux tube that requires a siphon flow of sufficient speed to allow a simple arched equilibrium path; if the flow is too slow, then there is no simple arched equilibrium path, but there is an alternative sinusoidal equilibrium path with the same flow speed at the central point $\bar{x} = 0$. For the sinusoidal equilibrium paths, which do not extend down to $\bar{h} = 0$, the value of $\bar{v}_0$ is somewhat irrelevant; it is perhaps better to think of the examples in Figure 6 as a sequence of flows with different specified values of the flow speed $\bar{v}$ at the central point $\bar{x} = 0$.

V. CONCLUSIONS

We have shown how to calculate the equilibrium path of a thin magnetic flux tube in a stratified, nonmagnetic atmosphere when the flux tube contains a steady siphon flow. The equilibrium path is affected by the siphon flow, but the

problem is decoupled in the thin flux tube approximation because the siphon

flow variables can be determined as functions of height $\bar{h}$ irrespective of the

actual equilibrium path $\bar{h}(\bar{x})$. The large-scale mechanical equilibrium of the

thin flux tube involves a balance among the magnetic buoyancy force, the net

magnetic tension force, and the inertial force (centrifugal force) due to the

siphon flow along a curved path.

In general, the equilibrium path of a static thin flux tube in an infinite

stratified atmosphere takes the form of a symmetric arch of finite width, with

the flux tube becoming vertical at either end of the arch. A siphon flow within

the flux tube increases the curvature of the arched equilibrium path, in order

that the net magnetic tension force can balance the inertial force of the flow,

which tries to straighten the flux tube. Thus, a siphon flow reduces the width of

the arched equilibrium path, with faster flows producing narrower arches.

The effect of the siphon flow on the equilibrium path is generally greater for

flux tubes of weaker magnetic field strength.

We have shown examples of the equilibrium for both isothermal and

adiabatic siphon flows in thin flux tubes in an isothermal external atmosphere.

For isothermal flows, the magnetic buoyancy is always positive, and the

equilibrium path $\bar{h}(\bar{x})$ always has downward curvature ($d^2\bar{h}/d\bar{x}^2 < 0$) and the

equilibrium path must be an arch of finite width. For adiabatic flows, adiabatic

cooling reduces the buoyancy of the flux tube and produces arches of

greater width than those with isothermal flows. In some cases adiabatic

cooling more than offsets the magnetic buoyancy effect and causes sections of

the flux tube to be heavier than its surroundings (negatively buoyant) and thus

to have upward curvature ($d^2\bar{h}/d\bar{x}^2 > 0$); this leads to the possibility of

sinusoidal equilibrium paths of infinite horizontal extent.

The isothermal and adiabatic siphon flows computed in Papers I and II

were based on an assumed equilibrium path in the form of a parabolic arch

of unspecified width. It turns out that the parabolic paths of the examples in

Papers I and II are very close to the true equilibrium path computed by the

methods of the present paper when we match the width of the arch in the two

cases. Thus, the examples in Papers I and II are fairly accurate as they stand

(within a few percent), with their assumed parabolic paths. However, since

the siphon flow variables actually depend only on the height $\bar{h}$ and not on its

distribution $\bar{h}(\bar{x})$, the flows computed in Papers I and II are precisely accurate

if, instead of associating them with the assumed parabolic paths, we associate

them with the exact equilibrium paths computed by the methods of the present

paper. This can be thought of as mapping the siphon flow along the parabolic

arch onto the true equilibrium arch by associating points of the same height $\bar{h}$.

The motivation for our study of siphon flows in isolated magnetic flux tubes

is the possible applications to magnetic structures in the solar atmosphere,

including intense photospheric flux tubes and sunspot penumbral filaments.

We have discussed these applications in some detail in Papers I and II. Here we note that in general the arched equilibrium paths of an isolated magnetic flux tube are fairly narrow, with footpoints separated horizontally by only some five to ten density scale heights (on the order of a thousand kilometers on the surface of the Sun). This short span of the flux-tube arch poses a problem for applications to penumbral filaments and intense photospheric flux tubes. Penumbral filaments are observed to extend horizontally over several thousand kilometers, for example. We have seen that adiabatic flows produce generally wider arches than isothermal flows, so to the extent that more realistic radiative flows allow some adiabatic cooling, somewhat wider arches may occur.

However, a more likely mechanism for allowing the wider arches observed on the Sun has to do with other "canopy" magnetic fields at higher levels in the external atmosphere. Although we have considered the equilibrium path of a single, isolated flux tube without regard to any other magnetic fields in the external atmosphere, on the Sun the atmosphere is generally filled with magnetic field above some height in the low chromosphere. In the case of a penumbral filament this field is the general spreading canopy of the overall sunspot magnetic field, and in the case of an intense flux tube in the quiet photosphere this field is the general canopy magnetic field covering the inter-network regions of the quiet Sun (Giovanelli

1980). We can imagine an isolated magnetic flux tube arching up to a point where it comes into contact with the overlying canopy field and then running horizontally for some distance along the base of the canopy before arching down again to the opposite footpoint (see also Thomas and Montesinos 1989). Along the section of the tube in contact with the canopy field, the mechanical equilibrium is established by a balance between the upward buoyancy of the flux tube and the downward magnetic pressure force due to the overlying canopy field. (Put another way, the isolated flux tube becomes part of the canopy field over this portion of the tube.) In this way, equilibrium arches (with flat tops) of much greater horizontal extent can occur on the Sun. The flow variables (velocity, cross-sectional area, etc.) will be quite uniform along the horizontal top of the arch in contact with the canopy, but in the isolated ascending and descending parts of the arch they will vary in the manner we have computed in this series of papers. Simple theoretical models of such extended equilibrium paths can be envisioned.

REFERENCES

Browning, P. K., and Priest, E. R. 1984, *Solar Phys.*, **92**, 173.

Browning, P. K., and Priest, E. R. 1986, *Solar Phys.*, **106**, 335.

Degenhardt, D. 1989, *Astr. Ap.*, **222**, 297.

Giovanelli, R. G. 1980, *Solar Phys.*, **68**, 49.

Montesinos, B., and Thomas, J. H. 1989, *Ap. J.*, **337**, 977 (Paper II).

Parker, E. N. 1975, *Ap. J.*, **201**, 494.

Parker, E. N. 1979, *Cosmical Magnetic Fields* (Oxford: Clarendon Press),

    sec. 8.6.

Press, W. H., Flannery, B. P., Teukolsky, S. A., and Vetterling, W. T. 1986,

    Numerical Recipes (Cambridge: Cambridge University Press), chap. 15.

Spruit, H. C. 1981, *Astr. Ap.*, **98**, 155.

Thomas, J. H. 1988, *Ap. J.* , **333**, 407 (Paper I).

Thomas, J. H. 1989, in *The Physics of Magnetic Flux Ropes*, ed. C. T. Russell,

    E. R. Priest, and C. Lee (Washington: American Geophysical Union), in

    press.

Thomas, J. H., and Montesinos, B. 1989, in *Proc. IAU Symp. No. 138, Solar*

    Photosphere: Structure, Convection, and Magnetic Fields, ed. J. O. Stenflo

    (Dordrecht: Reidel), in press.

Figure Captions

Fig. 1. Basic geometry of an arched thin magnetic flux tube, showing the coordinate system and the unit tangential and normal vectors σ and v.

Fig. 2. Plots of (a) the equilibrium path $\bar{h}(\bar{x})$, (b) the velocity $\bar{v}(\bar{x})$, (c) the cross-sectional area $\bar{A}(\bar{x})$, and (d) the plasma beta $\beta(\bar{x})$ for a thin magnetic flux tube containing isothermal siphon flows, with $\beta_0 = 3.0$ and $\alpha = 1.0$. Shown here are the static isothermal case (dot–dash curves), which is independent of β_0, and three examples of siphon flows: two subcritical flows (solid curves) and the critical flow (dashed curves) with both the subcritical (long dash) and supercritical (short dash) downstream branches. The specified values of $\bar{v}_0$ (the velocity at $\bar{h} = 0$) for the three siphon flows are 0.15, 0.25, and $\bar{v}_{0c} = 0.303440$. The corresponding maximum widths of the arch are $L_{max} = 6.05H$ and $5.69H$ for the purely subcritical flows and $L_{max} = 5.31H$ for the critical flow (with its subcritical downstream branch), which can be compared with the value $L_{max} = 2\pi H = 6.28H$ for the static case.

Fig. 3. Plots of (a) the equilibrium path $\bar{h}(\bar{x})$ and (b) the velocity $\bar{v}(\bar{x})$ and cross-sectional area $\bar{A}(\bar{x})$ of the flux tube for critical isothermal siphon

flows with $\alpha = 1.0$ and three different values of β_0: $\beta_0 = 2.0$ (*solid curves*),

$\beta_0 = 3.0$ (*dashed curves*), and $\beta_0 = 6.0$ (*dotted curves*). In each case both

the subcritical and supercritical downstream branches are shown. Also

shown for comparison is the static case (*dot–dashed curve*), which is

independent of β_0. The critical initial velocities for these flows are $\bar{V}_{0c} =$

0.339169, 0.303440, and 0.244038 and the maximum widths of the

arches (for the subcritical downstream branches) are $L_{max} = 5.68H$,

5.31H, and 4.67H for $\beta_0 = 2.0$, 3.0, and 6.0, respectively.

Fig. 4. (*a*) The equilibrium paths of static adiabatic flux tubes in an isothermal

external atmosphere, with $\alpha = 1.0$, $\tau = 1.0$ (i.e., $T_0 = T_{e0}$), and several

different values of β_0. For β_0 somewhere between 4.5 and 5.0, the flux

tube becomes negatively buoyant at the top of the arch, and the equilibrium

path for larger β_0 switches over to the sinusoidal shape represented

here by the cases $\beta_0 = 5.0$ and 6.0. The maximum width of the arch is L_{max}

$= 7.32H$, 8.94H, 12.27H, and 17.18H for $\beta_0 = 2.0$, 3.0, 4.0, and 4.5,

respectively. (*b*) Similar to Fig. 4*a*, but with $\alpha = 2.0$. Here the case $\beta_0 = 6.0$

has sections with upward concavity due to negative buoyancy on either

side of the arch, and in the case $\beta_0 = 7.0$ the equilibrium has switched over

to a sinusoidal path. The maximum width of the arch is $L_{max} = 8.17H$, 9.70H, and 15.69H for $\beta_0 = 2.0$, 3.0, and 6.0, respectively.

Fig. 5. Plots of (a) the equilibrium path $\bar{h}(\bar{x})$, (b) the velocity $\bar{v}(\bar{x})$, (c) the cross-sectional area $\bar{A}(\bar{x})$, and (d) the plasma beta $\beta(\bar{x})$ for cases of adiabatic siphon flows with $\alpha = 1.0$, $\beta_0 = 3.0$, and $\tau = 1.0$. Shown here are the static adiabatic case (dot-dashed curves), two examples of subcritical flows (solid curves), and the critical flow (dashed curves) with both its subcritical and supercritical downstream branches. The specified values of $\bar{v}_0$ (the velocity at $\bar{h} = 0$) for the three siphon flows are 0.15, 0.25, and $\bar{v}_{0c}$ = 0.316207. The corresponding maximum widths of the arch are $L_{max} =$ 8.60H and 7.94H for the two purely subcritical flows and $L_{max} = 7.11H$ for the critical flow (with the subcritical downstream branch), which can be compared with the value $L_{max} = 8.94H$ for the static case.

Fig. 6. Similar to Figures 5a,b, except with $\beta_0 = 6.0$. The critical flow (dashed curves, with $\bar{v}_{0c} = 0.228438$) and the faster subcritical flow (with $\bar{v}_0 = 0.20$) allow a simple arched equilibrium path of finite width. The maximum width of the arch is $L_{max} = 18.30H$ for $\bar{v}_0 = 0.20$ and $L_{max} = 11.18H$ for the critical flow (with the subcritical downstream branch). The slower subcritical flow

(with $\bar{v}_0 = 0.15$) and the static case (*dot–dashed curves*) do not allow a simple arched equilibrium path; instead, there is a sinusoidal–shaped equilibrium path with the appropriate flow speed at the center $\bar{x} = 0$. The four cases here may be thought of as a sequence of flows with increasing flow speeds at the central point $\bar{x} = 0$ ($\bar{v} = 0.0, 0.319, 0.481$, and 0.730, respectively, at $\bar{x} = 0$).

BENJAMIN MONTESINOS: Department of Theoretical Physics, 1 Keble Road,

Oxford OX1 3NP, England

JOHN H. THOMAS: 436 Lattimore Hall, University of Rochester, Rochester,

NY 14627

Figure 1

Figure 2a

$\alpha=1.0 \quad \beta_0=3.0$

$\bar{v}_0=\bar{v}_{0c}$
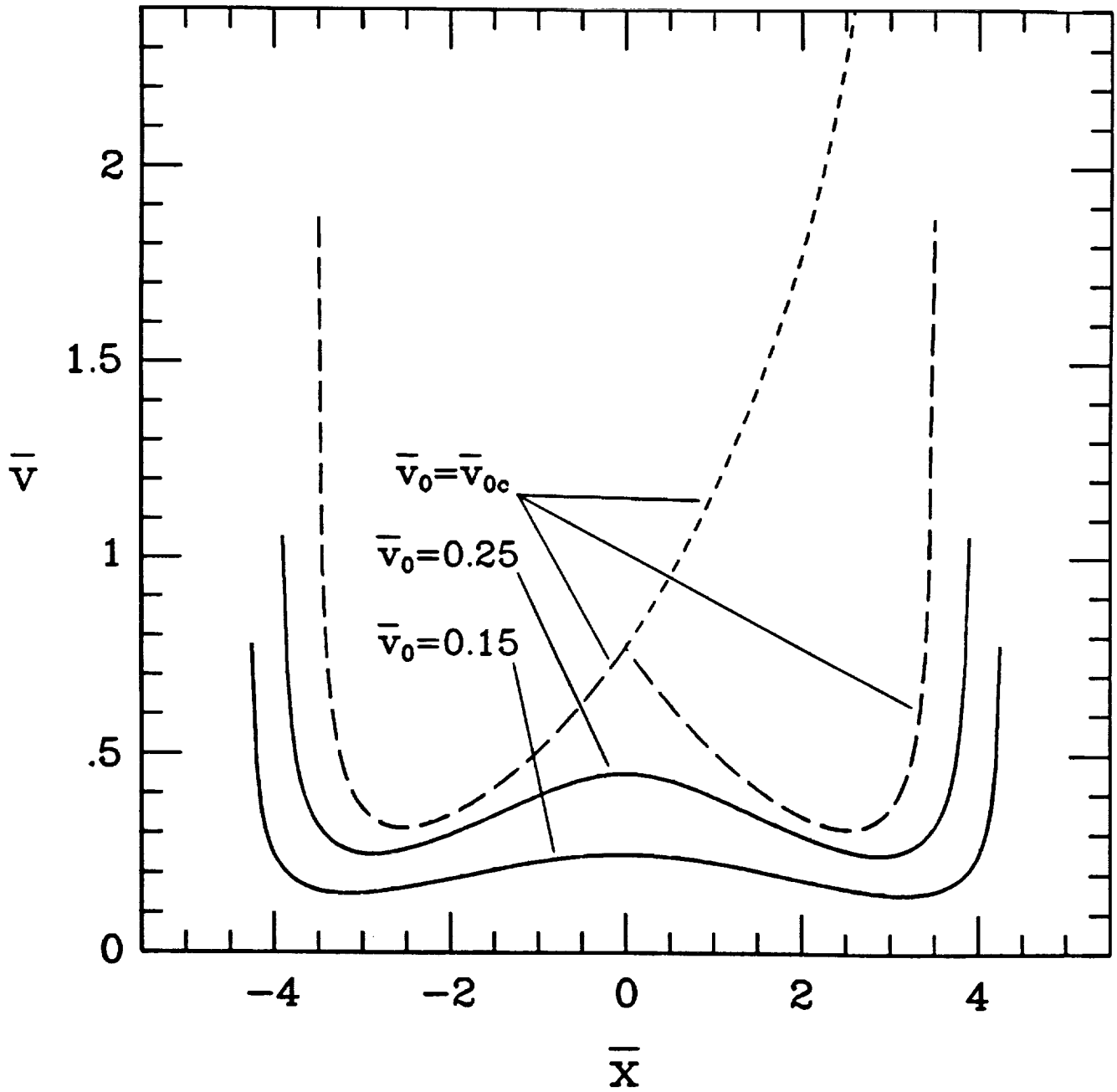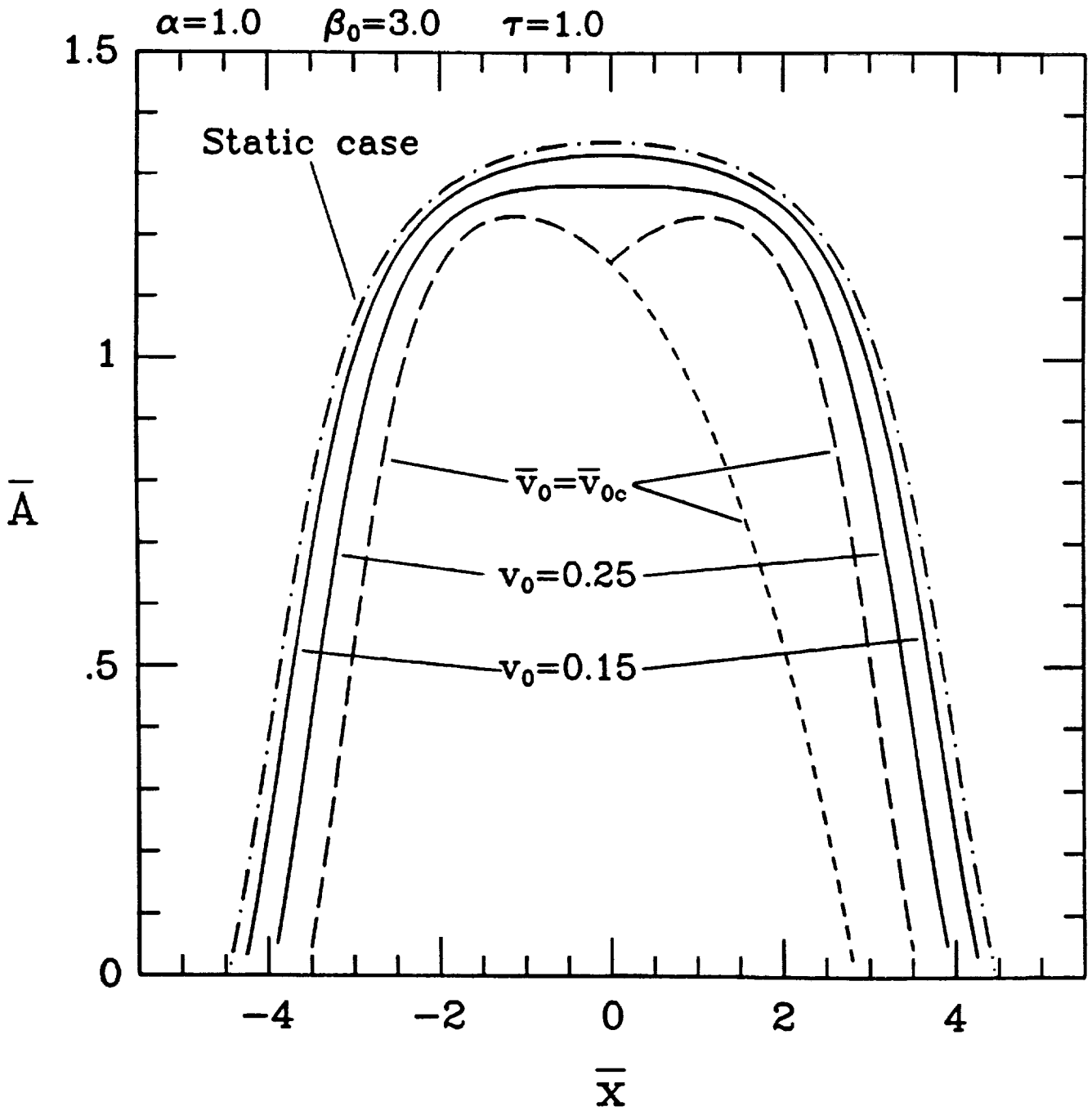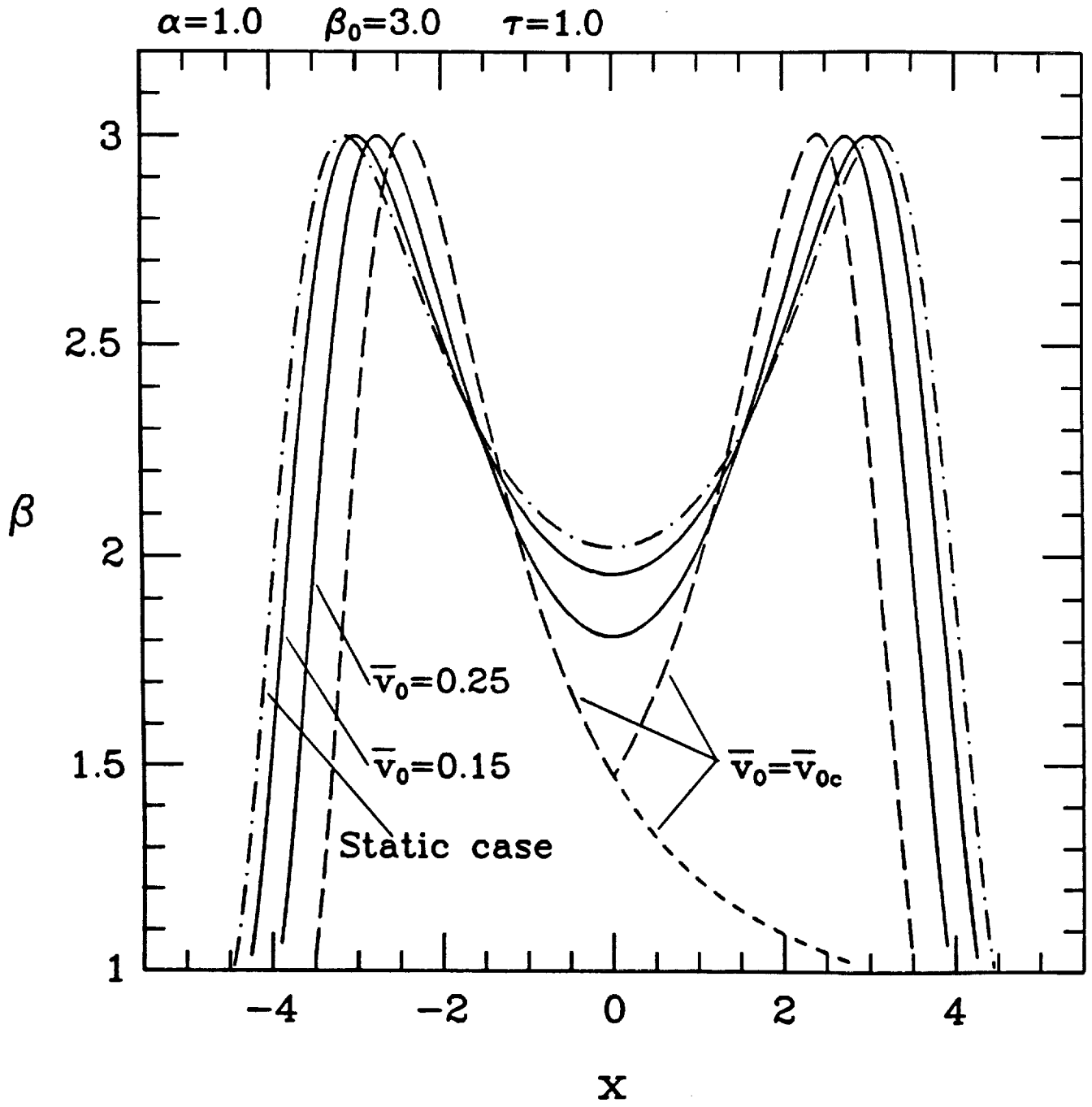
$\bar{v}_0=0.25$

$\bar{v}_0=0.15$
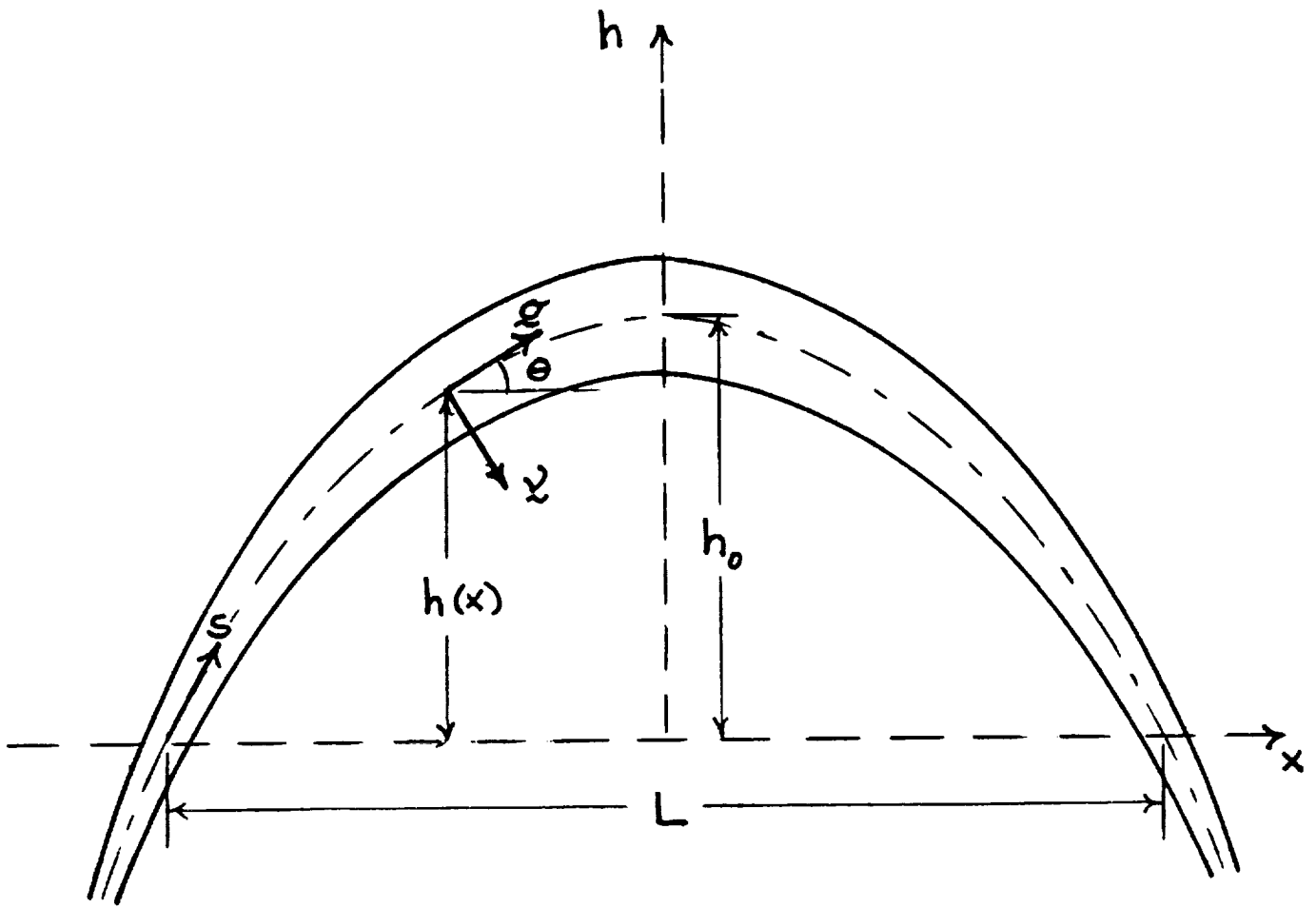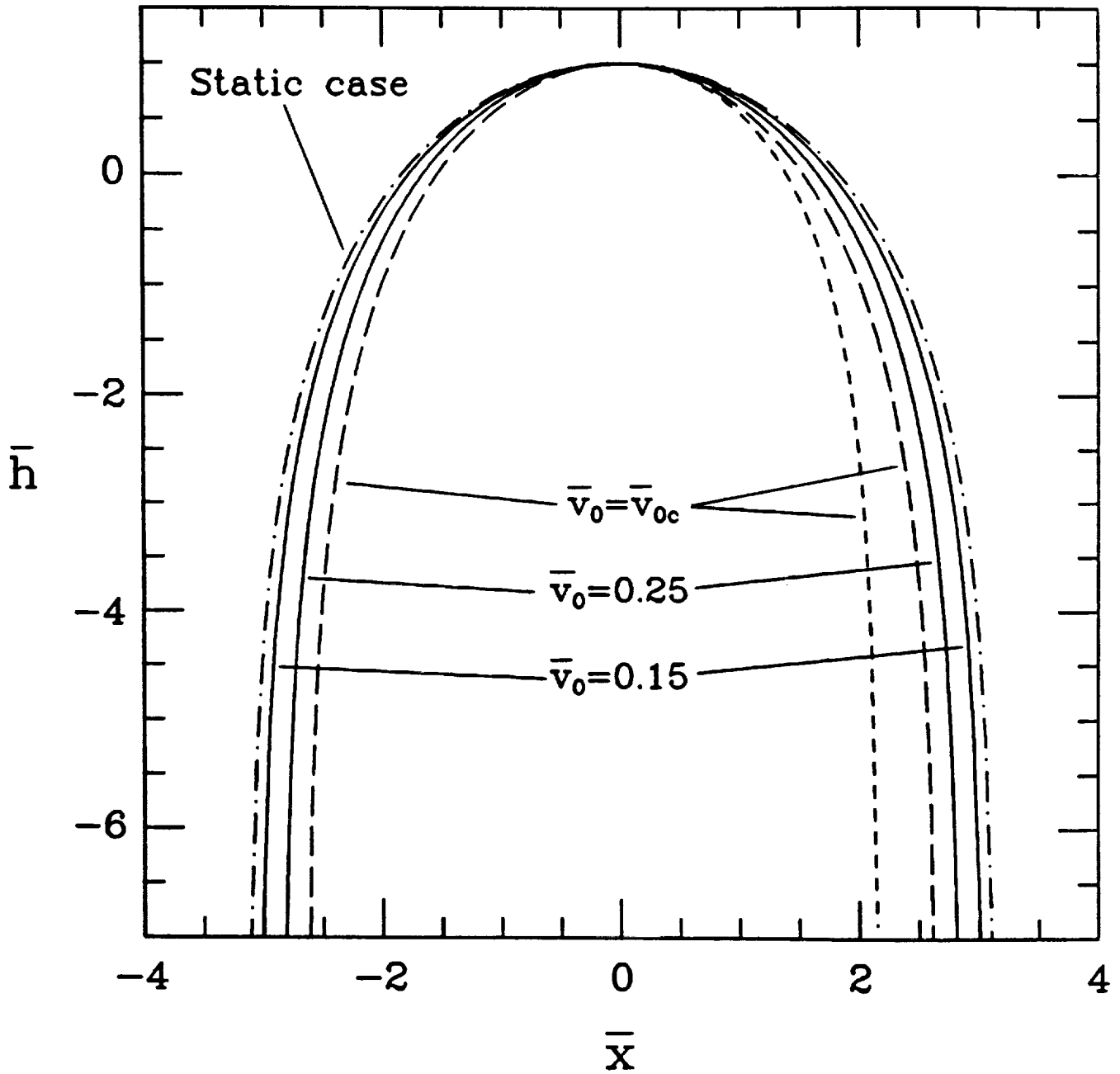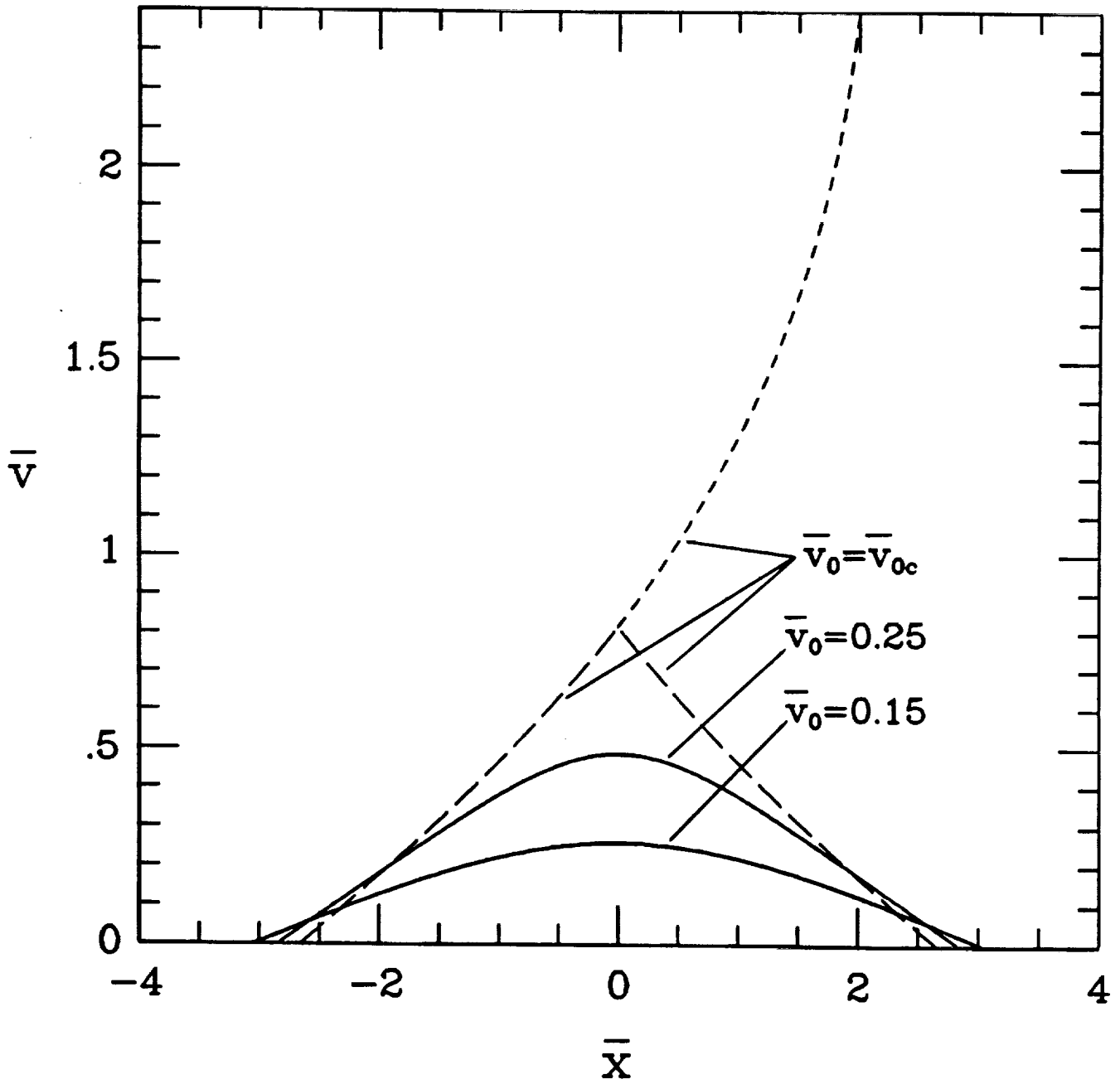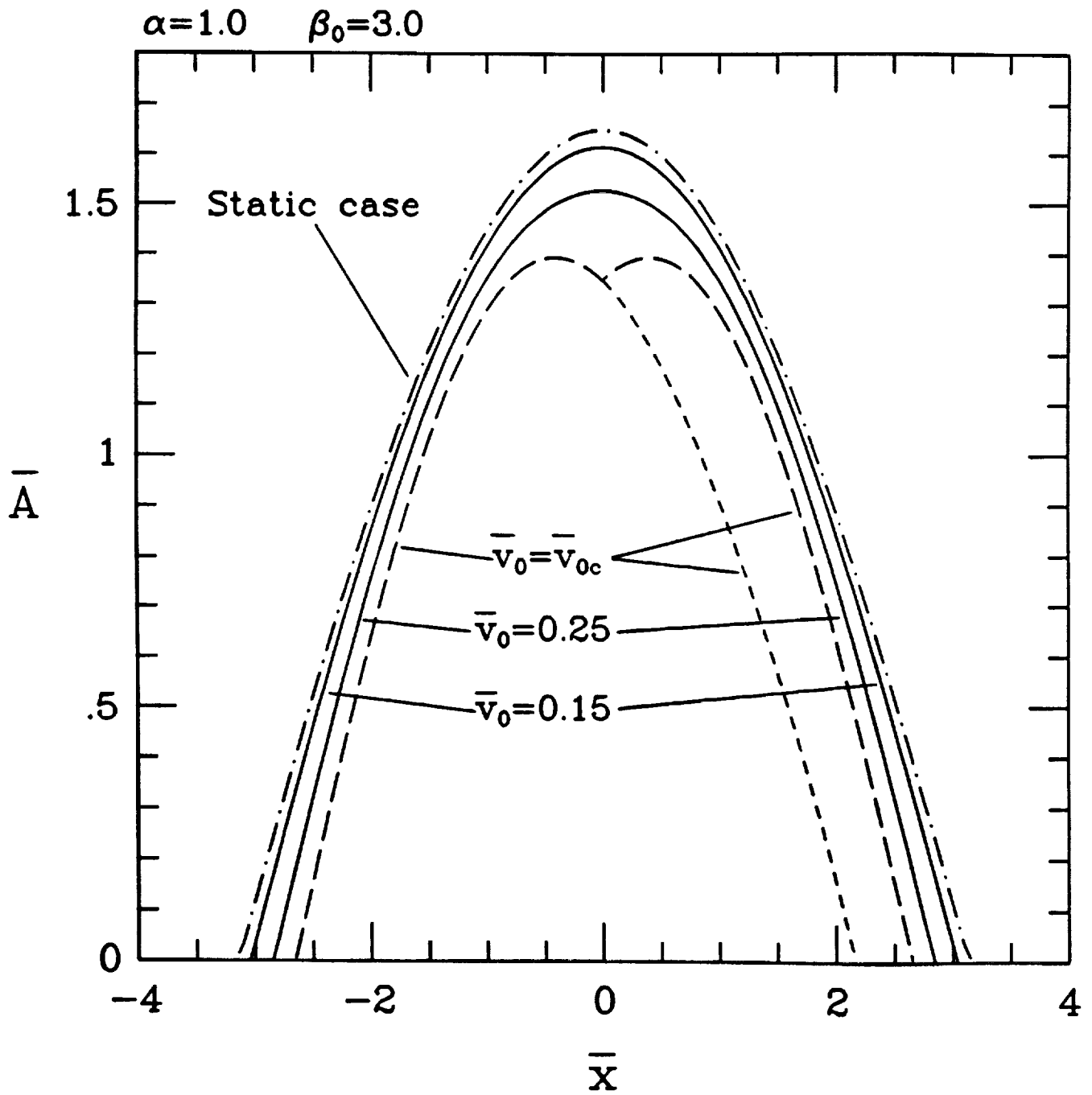
Figure 2b

Figure 2c
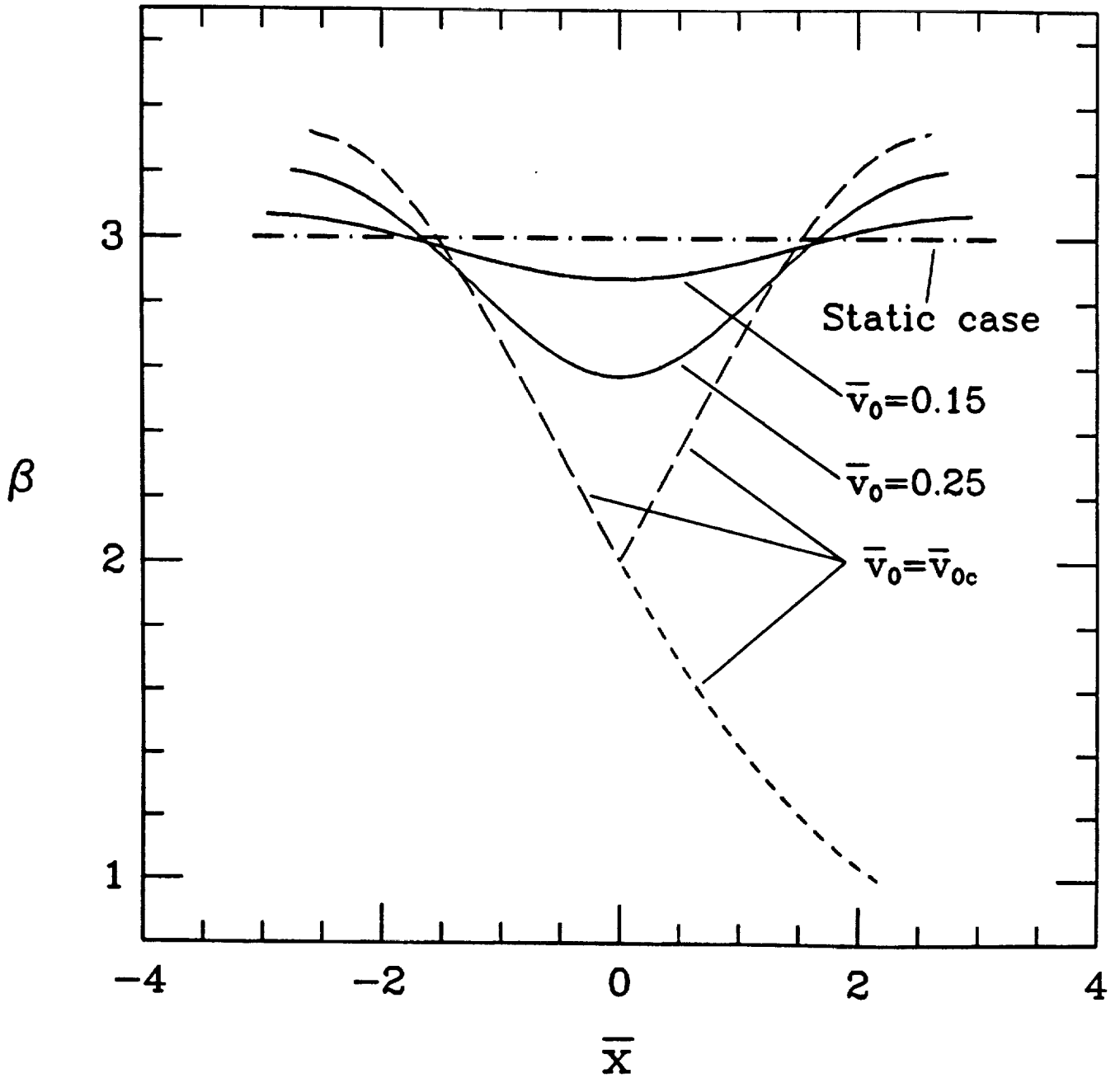
Figure 2d

Figure 3a

Figure 3b

α=1.0

Static case

β₀=2.0

β₀=3.0

β₀=6.0

Figure 4a

$\alpha=2.0 \quad \tau=1.0$

$\beta_0=8.0$

$\beta_0=7.0$

$\beta_0=6.0$

$\beta_0=3.0$

$\beta_0=2.0$

$\bar{h}$

$\bar{x}$

Figure 4b

Figure 5a

$\alpha = 1.0$ $\beta_0 = 3.0$ $\tau = 1.0$

$\overline{v}_0 = \overline{v}_{0c}$

$\overline{v}_0 = 0.25$

$\overline{v}_0 = 0.15$

$\overline{v}$

$\overline{x}$

Figure 5b

Figure 5c

$\alpha=1.0 \qquad \beta_0=3.0 \qquad \tau=1.0$

$\overline{v}_0=0.25$

$\overline{v}_0=0.15$

$\overline{v}_0=\overline{v}_{0c}$

Static case

Figure 5d

Figure 6a

$\alpha = 1.0 \quad \beta_0 = 6.0 \quad \tau = 1.0$

$\bar{v}_0 = 0.20$

$\bar{v}_0 = \bar{v}_{0c}$

$\bar{v}_0 = 0.15$

Figure 6b